Supporting Information

Flower-Shaped Self-Assembled $Ni_{0.5}Cu_{0.5}Co_2O_4$ Porous Architecture: A Ternary Metal Oxide as a High-Performance Charge Storage Electrode Material

Subhajyoti Samanta[†], Arpan Kumar Nayak[‡], Aniruddha Mukherjee[†], Debabrata Pradhan[‡], Biswarup Satpati[⊥], and Rajendra Srivastava[†]*

[†]Department of Chemistry, Indian Institute of Technology Ropar, Rupnagar-140001, India

[‡]Materials Science Centre, Indian Institute of Technology Kharagpur, Kharagpur, West Bengal-721302, India

[⊥]Surface Physics and Material Science Division, Saha Institute of Nuclear Physics, 1/AF, Bidhannagar, Kolkata 700 064, India

*Corresponding author Email: rajendra@iitrpr.ac.in (Dr. Rajendra Srivastava)

Contents

MATERIALS

All chemicals were of analytical reagent grade and used as received without further purification. NH_4F and Poly-vinyl alcohol (PVA) were purchased from Sigma Aldrich, India. Nickel chloride hexahydrate ($NiCl_2.6H_2O$), cobalt chloride hexahydrate ($CoCl_2.6H_2O$) and copper chloride tetrahydrate ($CuCl_2.4H_2O$) were obtained from Loba. Chemie. Pvt. Ltd., India. Poly(vinylidene difluoride) (PVDF) and 1-methyl-2-pyrrolidinone (NMP) were purchased from Alfa-Aesar. Urea was purchased from SD Fine Chemical Ltd., India. Graphite sheet was purchased from Nickunj Eximp. Enterprise Pvt. Ltd., Mumbai, India. Activated carbon (surface area ~ 2000 cm^2/g) was procured from MTI Corporation USA. Deionized water from Millipore Milli-Q system (Resistivity 18 MΩcm) was used in the electrochemical studies. Electrochemical measurements were performed in 3 M KOH solution. Breadboard, LED bulb and crocodile clips were bought from local market, Chandigarh, India.

MATERIALS CHARACTERIZATION

X-ray diffraction (XRD) patterns were recorded in the 2θ range of 5-80° with a scan speed of 2°/min on a PANalytical X'PERT PRO diffractometer, using Cu Kα radiation (λ=0.1542 nm, 40 kV, 40 mA). Nitrogen adsorption measurements were performed at -196 °C by Quantachrome Instruments, Autosorb-IQ volumetric adsorption analyzer. The sample was out-gassed at 200 °C for 3 h in the degassing port of the adsorption apparatus. The specific surface area of metal oxides was calculated from the adsorption data points obtained at P/P_0 between 0.05-0.3 using the Brunauer-Emmett-Teller (BET) equation. The pore diameter was estimated using the Barret-Joyner-Halenda (BJH) methods. Field emission scanning electron microscopy (FESEM) measurements were carried out on ZEISS Supra-40, Switzerland at an accelerating voltage of 5 kV to investigate the morphology of all the materials. SEM and EDAX of activated carbon were analyzed in a JEOL-6010, Japan SEM instrument operated at 30 kV. X-ray photoelectron spectroscopy (XPS) was carried out using an XPS system PHI 5000 VersaProbe II (ULVAC-PHI, INC, Japan) with a micro-focused (100 μm, 25 W, 15 kV) monochromatic Al-Kα source (hν = 1486.6 eV), a hemispherical analyzer and a multichannel detector. All binding energies were referenced to the C 1s peak at 284.8 eV of the surface adventitious carbon. Transmission electron microscopy (TEM) measurements were carried out using an FEI, Tecnai G2 F30-ST microscope operating at 300 kV. The same microscope is equipped with a scanning unit, an HAADF detector from Fischione (model 3000), and

energy dispersive X-ray spectroscopy (EDAX) attachments. The sample was dispersed in ethanol using an ultrasonic bath, and dispersed sample was mounted on a carbon coated Cu grid, dried, and used for TEM measurement. DRUV-visible spectra were recorded by Shimadzu (UV-2600) spectrophotometer. Microwave plasma atomic emission spectroscopy (MP-AES) measurements were performed using an Agilent G8003A instrument. To prepare MP-AES samples, materials were dissolved in 3 ml of 30 % HNO_3 inside an acid digester at 150 °C for 2 h.

Synthesis of MCo_2O_4

Briefly, 1 mmol $NiCl_2.6H_2O$/$CuCl_2.4H_2O$, 2 mmol $CoCl_2.6H_2O$, 12 mmol NH_4F, and 15 mmol urea were taken in 140 mL deionized water under magnetic stirring in an open flask. The stirring was continued for another 30 min till a viscous gel was formed. It was immediately transferred to a Teflon-lined autoclave and kept in an oven at 140 °C/9 h for hydrothermal treatment. Autoclave was cooled to ambient temperature, washed with de-ionized water and dried in an oven at 80 °C for overnight. The sample was then thermally annealed in a muffle furnace at 350 °C for 4 h at a heating rate of 5 °C/min.

ELECTROCHEMICAL MEASUREMENTS

The working electrode was fabricated by mixing the active electrode material powder of 95 wt % and 5 wt % of poly(vinylidenedifluoride) (PVDF) binder dissolved in 1-methyl-2-pyrrolidinone (NMP), making a slurry. Then the slurry was coated on a graphite sheet (1 cm^2 area) and dried in a vacuum oven at 120 °C for 2 h. The whole experiment was carried out in 3 M KOH solution. The electrochemical performances of the as-fabricated devices were studied on a CHI 760D electrochemical workstation by cyclic voltammetry (CV), galvanostatic charge-discharge (GCD) and electrochemical impedance spectroscopy (EIS) tests by using a three-electrode cell with platinum (Pt) foil as the counter electrode and a saturated calomel electrode (SCE) as the reference electrode.

Fabrication of Asymmetric Supercapacitor Device

For the fabrication of asymmetric supercapacitor device (ASCD), ternary metal oxide $Ni_{0.5}Cu_{0.5}Co_2O_4$ was used as positive electrode and activated carbon as negative electrode. Poly-vinyl alcohol (PVA) was taken in water (1:10 mL) and heated in 70 °C until a clear suspension was obtained under stirring condition. A separately prepared 2 M KOH solution was drop-wise added to this PVA suspension resulting in the formation of a gel electrolyte. A

whatman filter paper was soaked into this gel, sandwiched between two electrodes, and then dried at 60 °C for 6 h. The two electrodes setup was further analyzed for electrochemical measurements through CV, GCD, and EIS analysis. Four cells with identical mass loading were connected in a series and the whole assembly was charged through AUTOLAB 302N Galvanostat instrument with an applied current density of 10 A/g in the total potential window of 5.6 V (1.4 V each). Once the charging was completed, it was stopped and then connected to a red LED light via breadboard.

Table 1 Physico-chemical properties of all the electrode materials investigated in this study.

Electrode material	**Surface area (m^2/g)**	**Total pore volume (cc/g)**	**Co (wt %)**	**Cu (wt %)**	**Ni (wt %)**
$NiCo_2O_4$	73	0.25	48.8	-	24.6 (0.419 mol %)
$CuCo_2O_4$	64	0.32	48.1	25.5 (0.42 mol %)	-
$Ni_{0.5}Cu_{0.5}Co_2O_4$	120	0.35	48.4	12.8 (0.202 mol %)	12.3 (0.209 mol %)

Values presented in the parenthesis are metal content in mol%.

Table S2 Comparison of specific capacitance for $Ni_{0.5}Cu_{0.5}Co_2O_4$ with several Ni and Cu based spinel materials reported in literature.

S. No.	Electrode material	Synthetic method	Morphology	Electrode substrate	Electrolyte / concentration	C_{sp} (at 1 $A.g^{-1}$)	Surface area	Reference
1.	$CuCo_2O_4$	Urea-based precipitation	Irregular cauliflower-like microstructures	Nickel Foam	aq. KOH / 3(M)	338$F.g^{-1}$	13.5 $m^2.g^{-1}$	[1]
2.	$NiCo_2O_4$	Electro-deposition	Nanosheets	F-doped SnO_2	aq. KOH / 1(M)	506 $F.g^{-1}$	227.3 $m^2.g^{-1}$	[2]
3.	$CuCo_2O_4$ @MnO_2	Two-step solvothermal	Layered $CuCo_2O_4$ nanosheets@ MnO_2 nanoflakes	Nickel Foam	aq. Na_2SO_4 / 1(M)	416 $F.g^{-1}$	-	[3]
4.	$NiCo_2O_4$	Solvothermal	Nanoplate	Nickel Foam	1 M KOH	297 $F.g^{-1}$	67.2 $m^2.g^{-1}$	[4]
5.	$NiCo_2O_4$	Polymer-assisted solution method	coral reefs	Nickel mesh	1 M KOH	217 $F.g^{-1}$	5.7 $m^2.g^{-1}$	[5]
6.	$NiCo_2O_4$	Solid state annealing	Nanorod (TEM)	Nickel mesh	2 M KOH	565 $F.g^{-1}$	71.46 $m^2.g^{-1}$	[6]
7.	CuO/$CuCo_2O_4$ nanocomposite	Solution followed by Microwave	Nanorod like	Graphite Sheet	1 M KOH	359 $F.g^{-1}$	-	[7]
8.	Dopamine doped $NiCo_2O_4$	Precipitation followed by thermal annealing	Flower/leaf like	Nickel foil	2 M KOH	600 $F.g^{-1}$ at 5 A/g	59 $m^2.g^{-1}$	[8]
9.	Hierarchical $NiCo_2O_4$ nanosheets@hollow microrod arrays	Electro-deposition	nanosheets@ hollow microrod	Nickel Foam	1 M KOH	678 $F.g^{-1}$ at 6 A/g	-	[9]

10.	Ni-CO oxide	Chemical bath deposition flowed by annealing	Flower like	Nickel Foam	1 M KOH	60 $F.g^{-1}$	135 $m^2.g^{-1}$	[10]
11.	$Ni_{0.5}Cu_{0.5}Co_2O_4$	Solvothermal	Flower-like hierarchical structure with nanorod assembly	Graphite Sheet	3 M KOH	367.4 $F.g^{-1}$	120 $m^2.g^{-1}$	This work

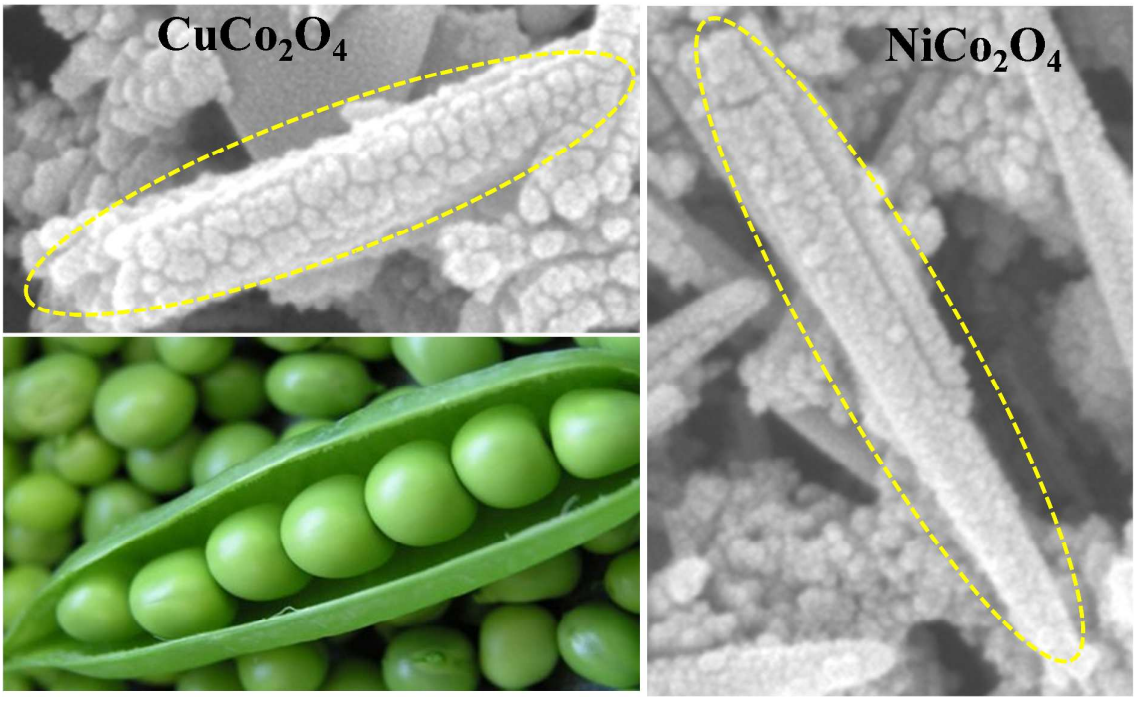

Figure S1 Representative FESEM images of $CuCo_2O_4$ and $NiCo_2O_4$ that resemble with a natural peapod.

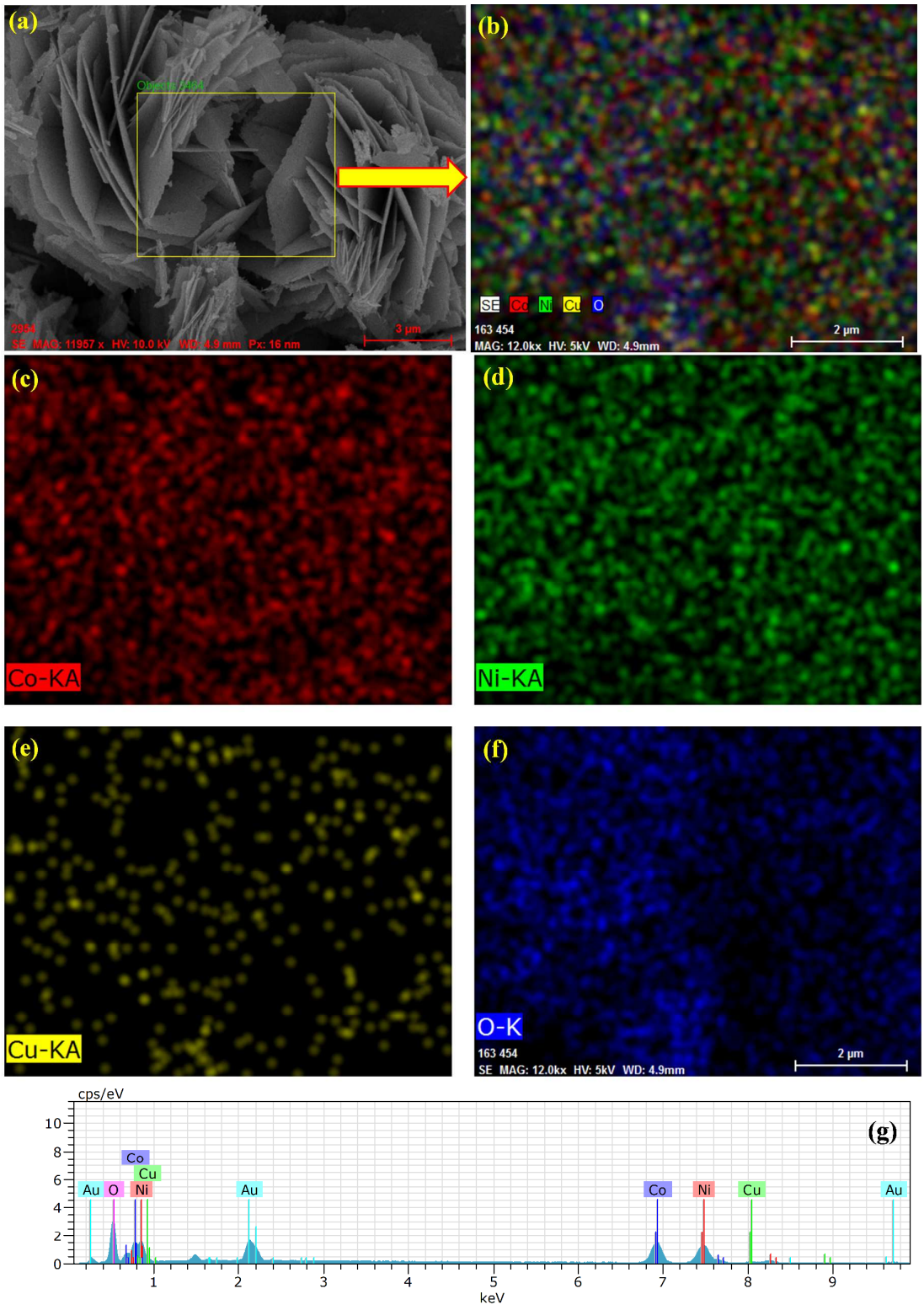

Figure S2 (a) FESEM images of $Ni_{0.5}Cu_{0.5}Co_2O_4$, (b) Mapping for all the elements in selected area in the FESEM images, its individual elemental mapping of (c) Co, (d) Ni, (e) Cu, (f) O, and (g) EDAX profile from the selected area shown in "a".

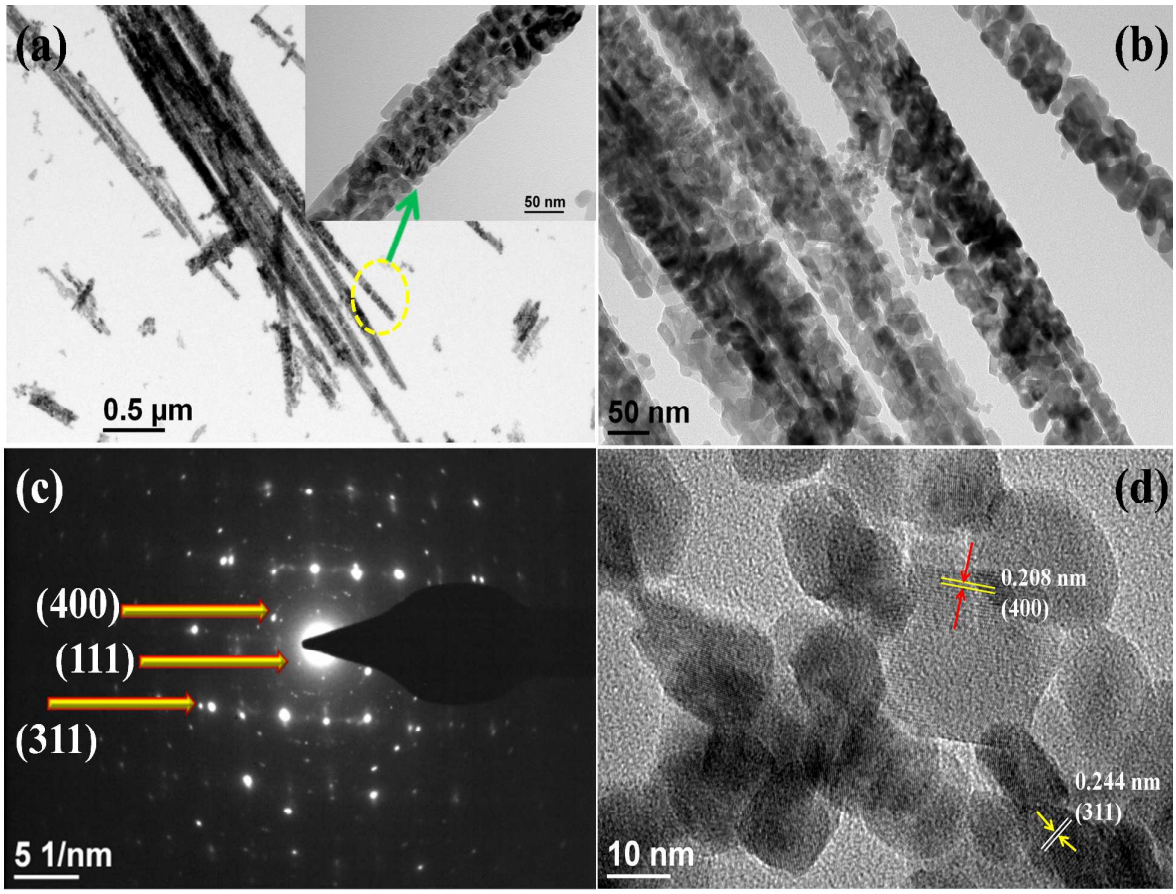

Figure S3 (a-b) TEM images, (c) SAED pattern, and (d) HRTEM images of $CuCo_2O_4$.

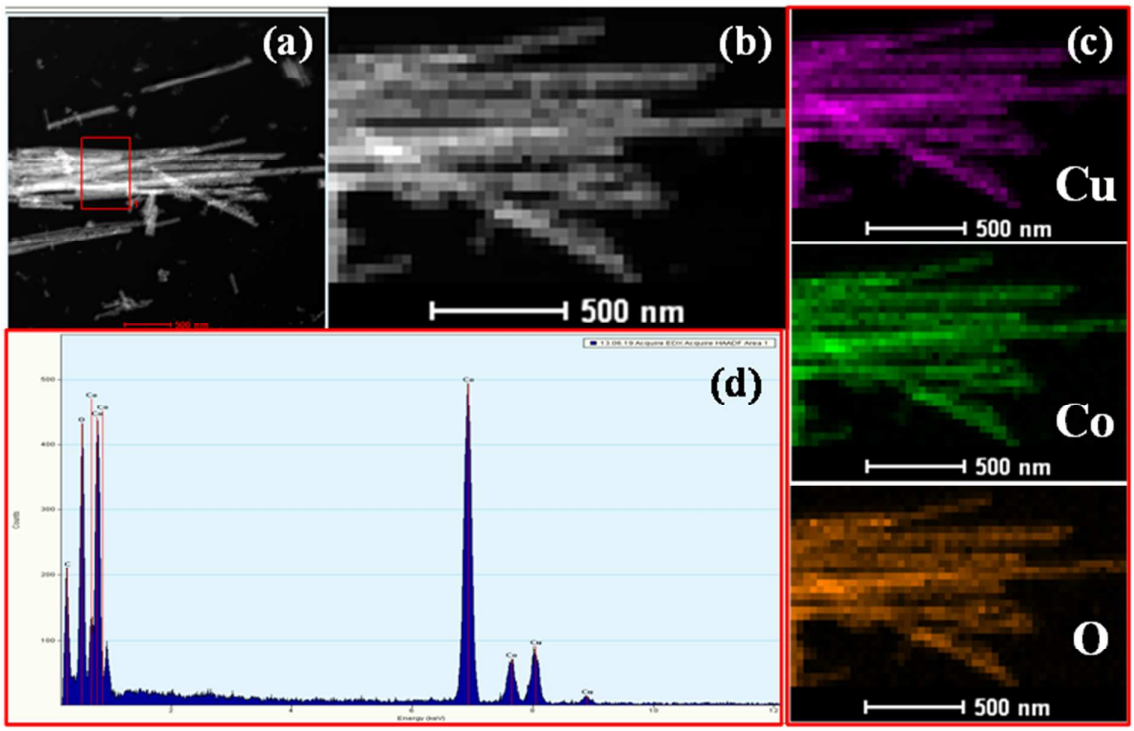

Figure S4 (a) STEM-HAADF image, (b) Drift corrected image, (c) elemental mapping of individual elements from the marked area of panel "a", and (d) its corresponding EDAX from the marked area of panel "a" for $CuCo_2O_4$.

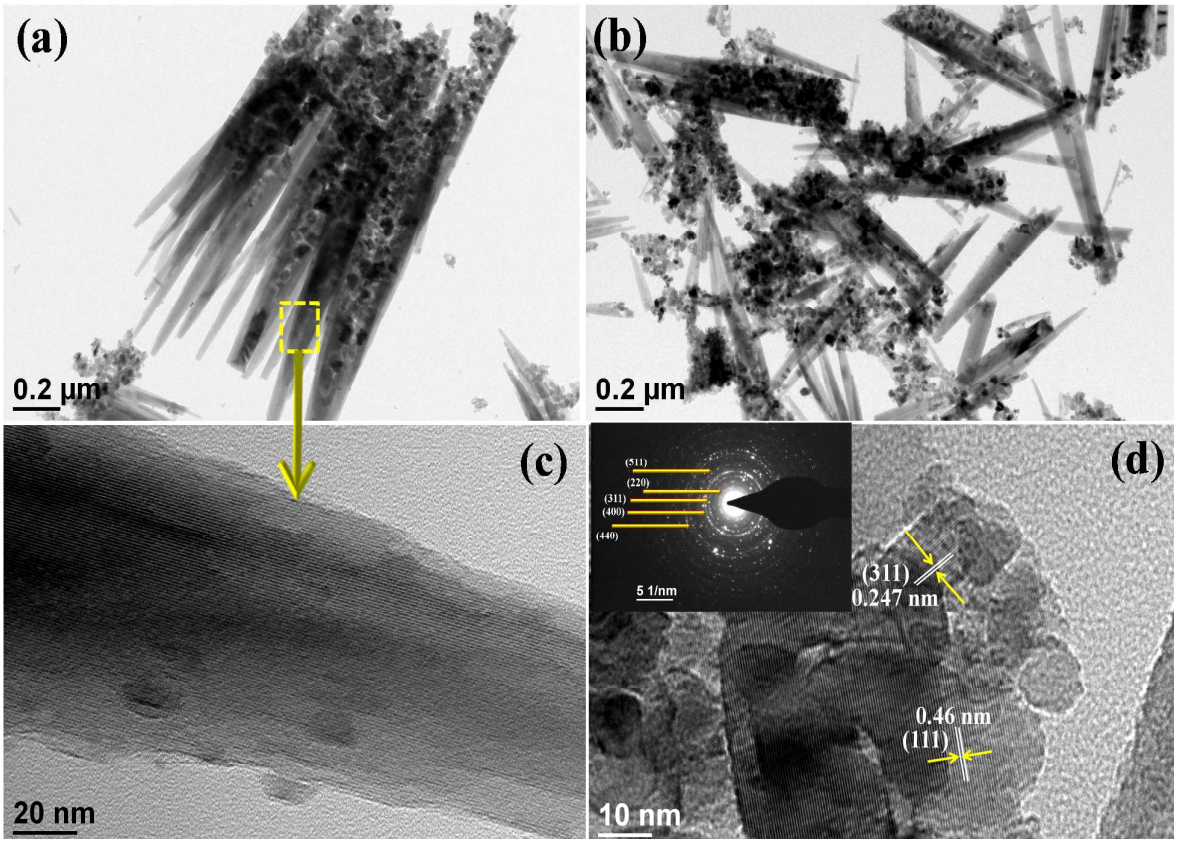

Figure S5 (a-c) TEM images and (d) HRTEM images of $NiCo_2O_4$ (Inset shows the SAED pattern).

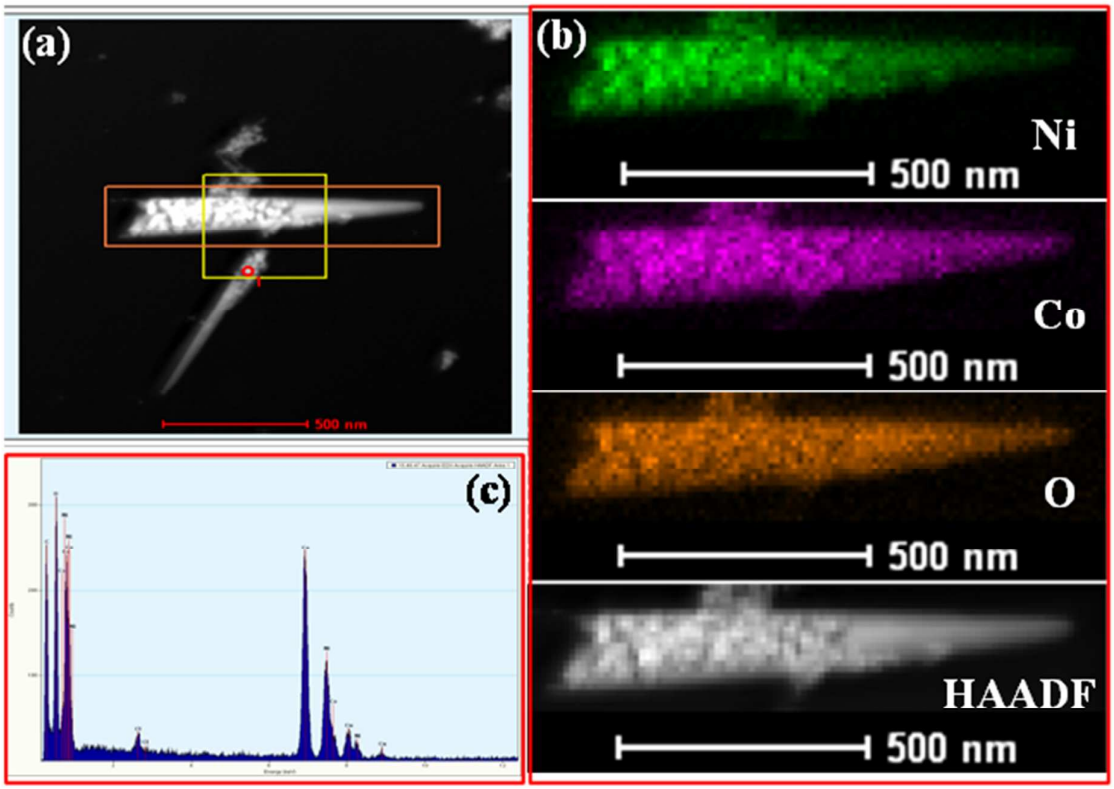

Figure S6 (a) STEM-HAADF image, (b) mapping of individual elements from the marked orange area in the panel "a", and (c) its corresponding EDAX from the marked yellow area in the panel "a" for $NiCo_2O_4$.

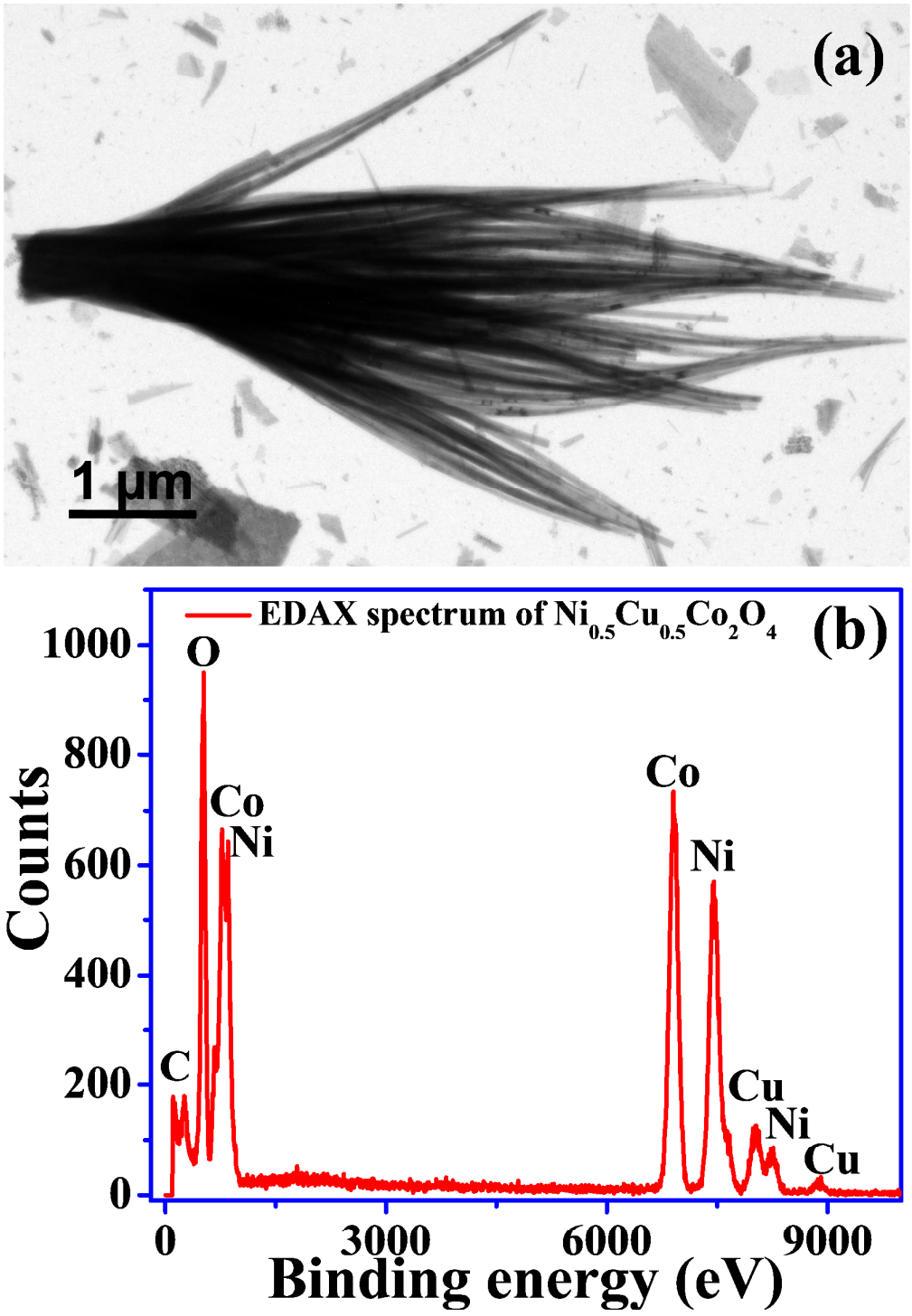

Figure S7 (a) Representative TEM images and (b) EDAX spectrum of flower-like $Ni_{0.5}Cu_{0.5}Co_2O_4$.

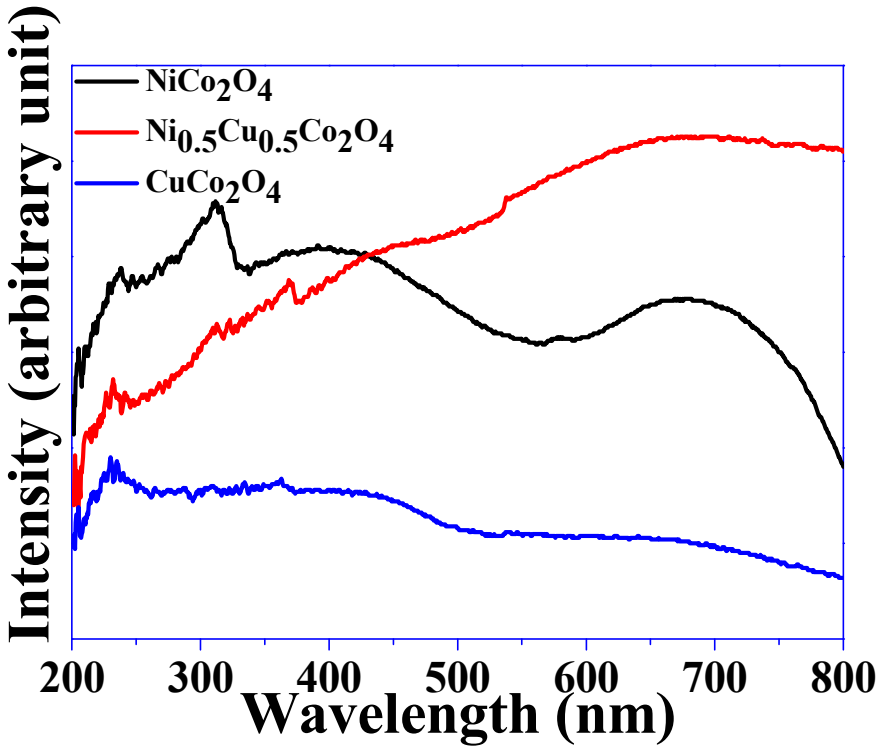

Figure S8 DRUV-visible spectra of all the materials synthesized in this investigation.

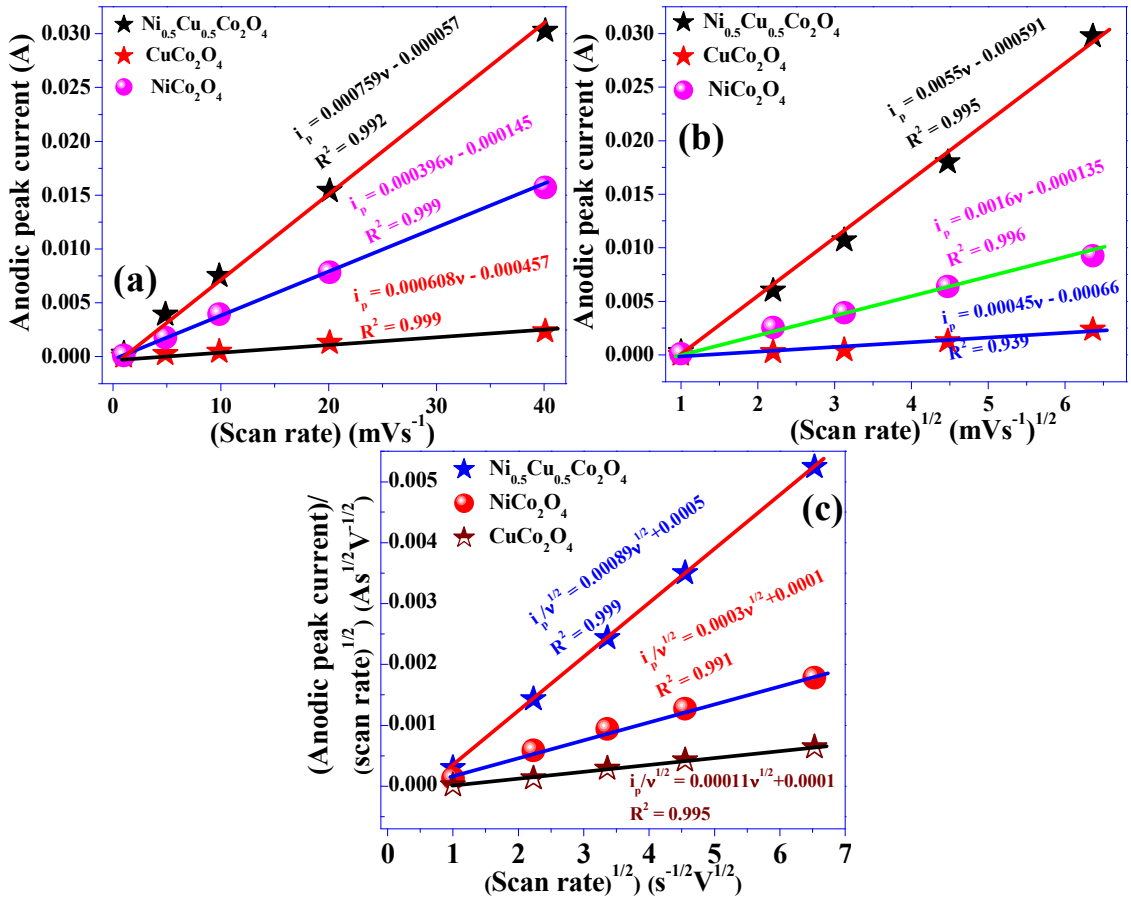

Figure S9 Plots (a) Anodic peak current *vs* scan rate, (b) Anodic peak current *vs* (scan rate)$^{1/2}$, and (c) $i_p/v^{1/2}$ *vs* $v^{1/2}$ of $NiCo_2O_4$, $CuCo_2O_4$, and $Ni_{0.5}Cu_{0.5}Co_2O_4$.

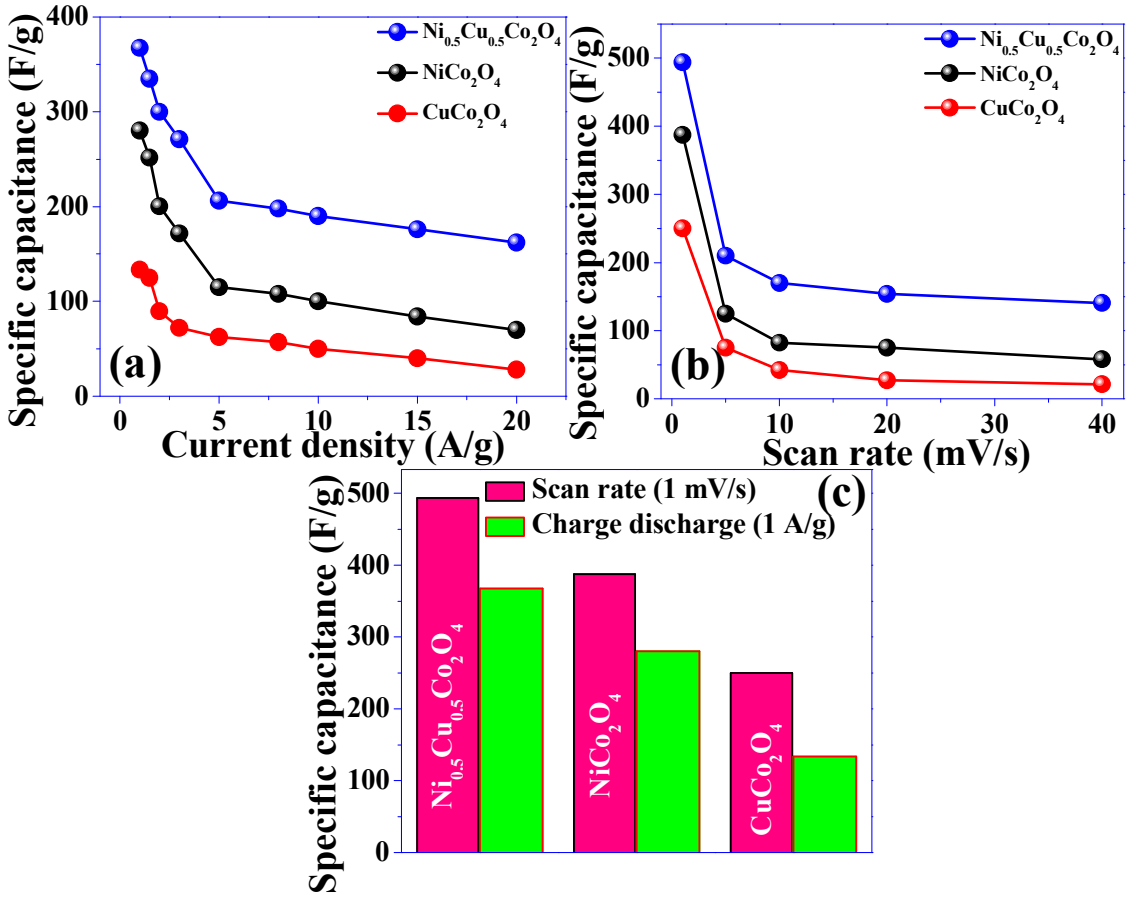

Figure S10 Specific capacitance as a function of (a) Applied current density (1-20 A/g) and (b) scan rate(1-40 mV/s) for $NiCo_2O_4$, $CuCo_2O_4$, and $Ni_{0.5}Cu_{0.5}Co_2O_4$, (c) Comparison in the specific current density at a scan rate of 1 mV/s and 1 A/g for $NiCo_2O_4$, $CuCo_2O_4$, and $Ni_{0.5}Cu_{0.5}Co_2O_4$.

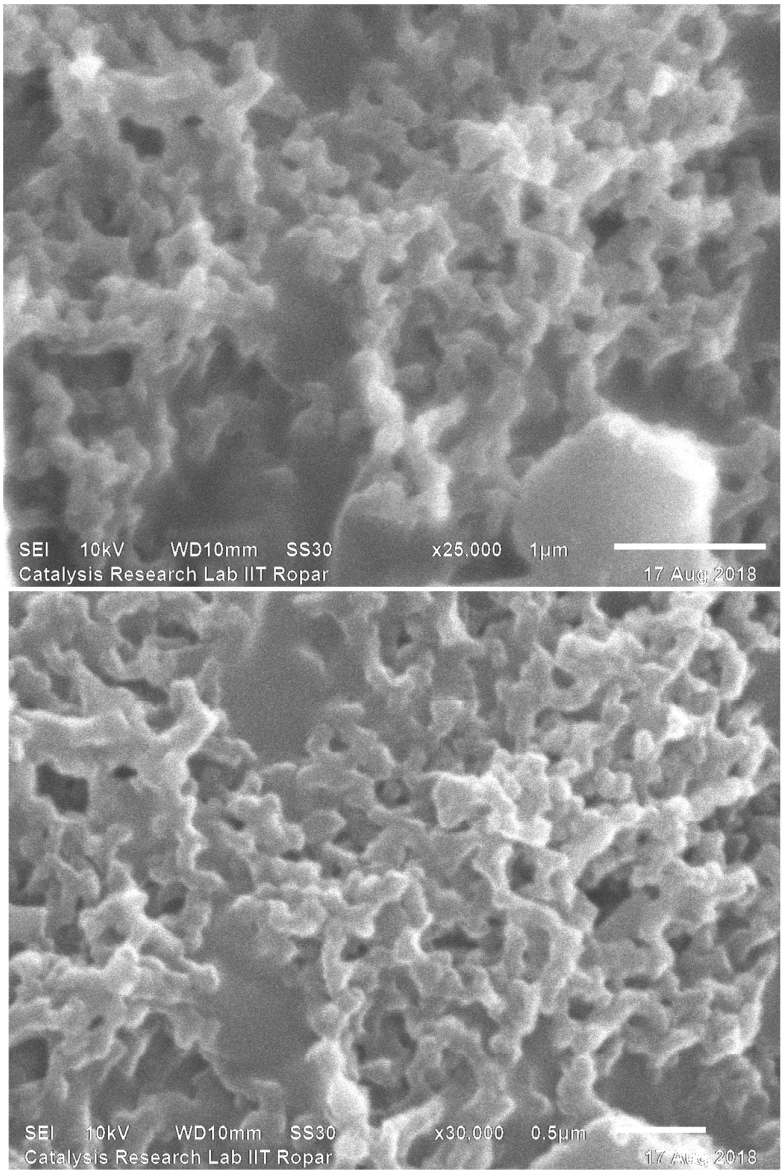

Figure S11 SEM images of activated carbon.

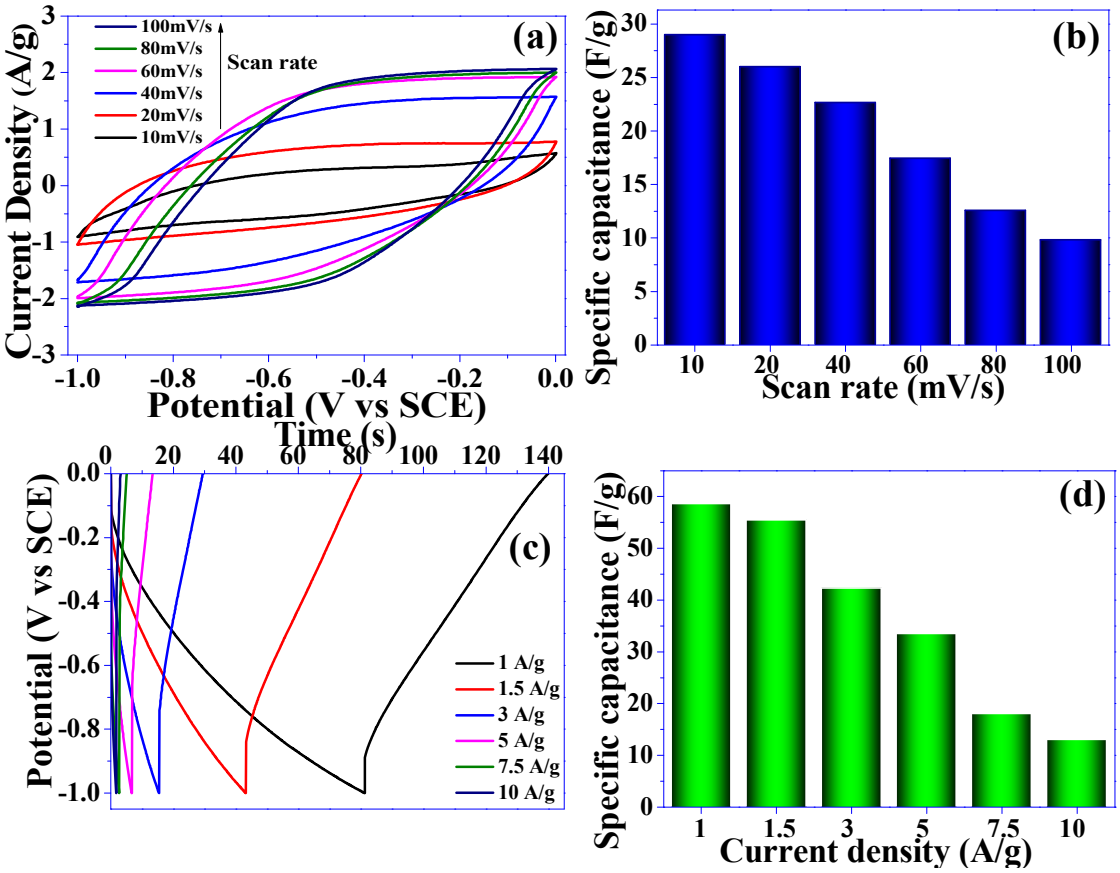

Figure S12 (a) CVs of activated carbon in 3 M KOH at various scan rate in the potential window 1.0 V, (b) Corresponding specific capacitance, (c) Galvanostatic charge-discharge profiles at various applied current densities, and (d) Corresponding specific capacitance.

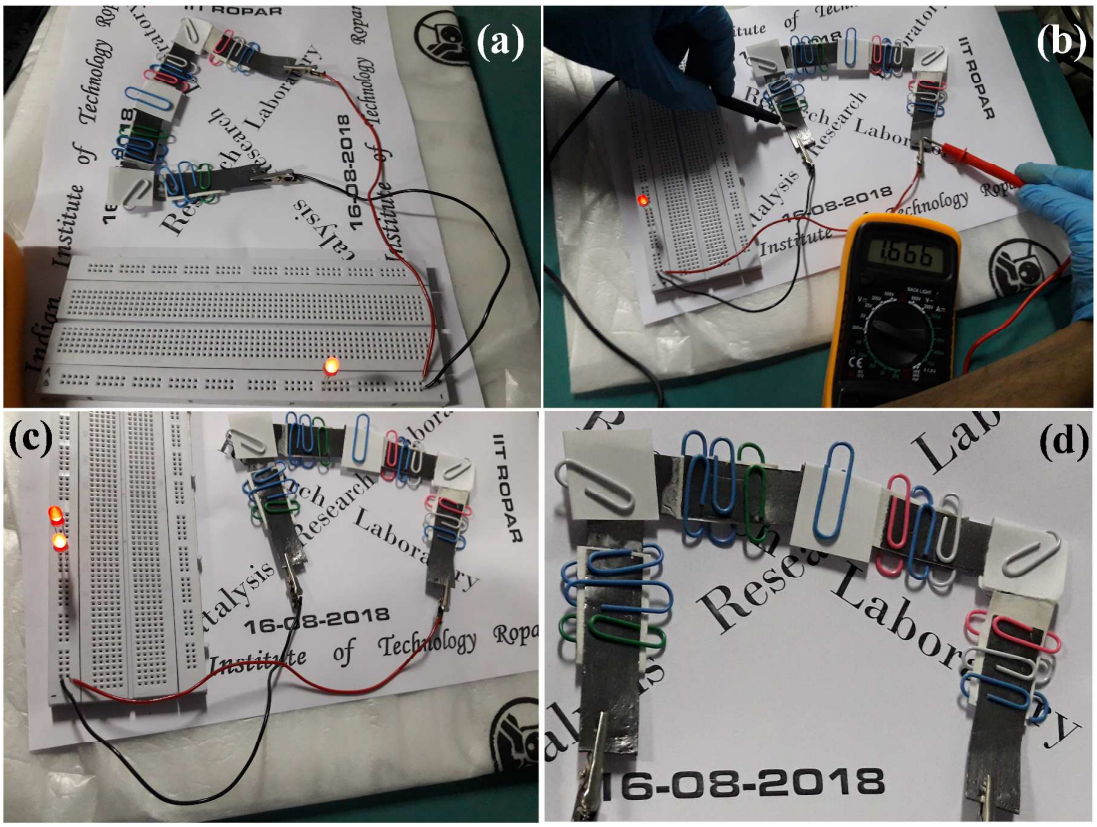

Figure S13 Digital photographs of configured full cell device (series connection of 4 single cell of identical mass loading) with activated carbon as negative electrode and $Ni_{0.5}Cu_{0.5}Co_2O_4$ as positive electrode connected (a) To a red LED bulb, (b) Obtained potential output after charging, (c) Two red LED bulbs, and (d) Enlarge snap of the configured device.

REFERENCES

(1) Pendashteh, A.; Rahmanifar, M. S.; Kaner, R. B.; Mousavi, M. F. Facile Synthesis of Nanostructured $CuCo_2O_4$ as a Novel Electrode Material for High-Rate Supercapacitors. *Chem. Commun*. **2014**, *50*, 1972-1975.

(2) Lu, X.; Huang, X.; Xie, S.; Zhai, T.; Wang, C.; Zhang, P.; Yu, M.; Li, W.; Liang, C.; Tong, Y. Controllable Synthesis of Porous Nickel-Cobalt Oxide Nanosheets for Supercapacitors. *J. Mater. Chem.* **2012**, *22*, 13357-13364.

(3) Kuang, M.; Liu, X. Y.; Dong, F.; Zhang, Y. X. Tunable Design of Layered $CuCo_2O_4$ Nanosheets@MnO_2 Nanoflakes Core-Shell Arrays on Ni Foam for High-Performance Supercapacitors. *J. Mater. Chem. A* **2015**, *3*, 21528-21536.

(4) Pu, J.; Wang, J.; Jin, X.; Cui, F.; Sheng, E.; Wang, Z. Porous Hexagonal $NiCo_2O_4$ Nanoplates as Electrode Materials for Supercapacitors. *Electrochim. Acta* **2013**, *106*, 226-234.

(5) Wu, Y. Q.; Chen, X. Y.; Ji, P. T.; Zhou, Q. Q. Sol-Gel Approach for Controllable Synthesis and Electrochemical Properties of $NiCo_2O_4$ Crystals as Electrode Materials for Application in Supercapacitors. *Electrochim. Acta* **2011**, *56*, 7517-7522.

(6) Zhu, Y.; Pu, X.; Song, W.; Wu, Z.; Zhou, Z.; He, X.; Lu, F.; Jing, M.; Tang, B.; Ji. X. High capacity $NiCo_2O_4$ Nanorods as Electrode Materials for Supercapacitor. *J Alloys Compd.* **2014**, *617*, 988-993.

(7) Shanmugavani, A.; Selvan, R. K. Improved Electrochemical Performances of $CuCo_2O_4$/CuO Nanocomposites for Asymmetric Supercapacitors. *Electrochim. Acta* **2016**, *188*, 852-862.

(8) Veeramani, V.; Madhu, R.; Chen, S-M.; Sivakumar, M. Flower-Like Nickel-Cobalt Oxide Decorated Dopamine-DerivedCarbon Nanocomposite for High Performance Supercapacitor Applications. *ACS Sustainable Chem. Eng.* **2016**, *4*, 5013-5020.

(9) Senthilkumar, S. T.; Kalai Selvan, R. Fabrication and Performance Studies of a Cable-type Flexible Asymmetric Supercapacitor. *Phys. Chem. Chem. Phys.* **2014**, *16*, 15692-15698.

(10) Tang, C.; Tang, Z.; Gong, H. Hierarchically Porous Ni-Co Oxide for High Reversibility Asymmetric Full-Cell Supercapacitors. *J. Electrochem. Soc.* **2012**, *159*, A651-A656.